A Complete Modeling and Simulation of Induction Generator Wind Power Systems

Yu Zou Malik Elbuluk* Yilmaz Sozer
Department of Electrical and Computer Engineering
University of Akron
Akron, OH 44325-3904
*melbuluk@uakron.edu

***Abstract* –This paper presents the modeling and simulation of wind power systems based on two different induction generators; the squirrel-cage induction generator (SCIG) and the doubly-fed induction generator (DFIG). The techniques of direct grid integration of SCIG system and independent power control of DFIG system are discussed. Particularly, to solve the droop in distribution line voltage in SCIG system, a reactive power static compensator (STACOM) is used and a comparison of distribution line voltage is conducted between the SCIG and DFIG systems. Besides, in DFIG system, a fitting curve for optimal power versus speed is proposed for the turbine model and a cross-coupling relation between three phase choke and stator-side converter is also emphasized. Both wind power systems and their grid integration techniques are modeled and simulated in Matlab/Simulink. The results demonstrated the characteristics of both systems under varying wind speeds. Compared to the conventional constant speed SCIG system, variable speed DFIG reveals its superiority in terms of optimal power capture as well as constant distribution line voltage.**

I. Introduction

The increasing emphasis on renewable wind energy has given rise to augmented attention on more reliable and advantageous electrical generator systems. Induction generator systems have been widely used and studied in wind power system because of their advantages over synchronous generators, such as smaller size, lower cost and lower requirement of maintenance [1][2]. The straightforward power conversion technique using SCIG is widely accepted in fixed speed applications with less emphasis on the high efficiency and control of power flow. However, such direct connection with grid would allow the speed to vary in a very narrow range and thus limit the wind turbine utilization and power output. Another major problem with SCIG power system is the source of reactive power, that is, an external reactive power compensator is required to hold distribution line voltage and prevent whole system from overload. On the other hand, DFIG with variable speed ability has higher energy capture efficiency and improved power quality, and thus has attracted more attentions. With the advent of power electronics, a back-to-back converter, which consists of two bidirectional converters and a dc-link, acts as an optimal operation tracking interface between generator and the grid [3][4][5]. Field orientation control (FOC) is applied to both rotor- and stator-side converters to achieve desirable control on voltage and power [6][7].

This paper presents the modeling of SCIG and DFIG wind systems, including the turbine, the FOC of converters, and connection to the grid. A STACOM is applied to SCIG system to reduce voltage droop in distribution line. Comparison between SCIG with and without STACOM, as well as DFIG system clearly showed different results in the distribution line voltage. The paper is organized as follows: In section II, the wind turbine mathematical model is described and an expression of optimal output power versus rotor speed is proposed. In section III, the SCIG wind power system is established. The mathematical model of the DFIG is introduced in section IV. Generally, the FOC was presented based on DFIG mathematical equations only. However, since a three phase choke is commonly used to couple stator-side converter into grid, this paper proposes the FOC schemes of stator-side converter involving the choke and it turns out that both stator- and rotor-side converter voltages consist of a current regulation part and a cross-coupling part. Finally, the steady-state and dynamic simulation results are presented and discussed in section V.

II. Wind Turbine

Wind energy is extracted through wind turbine blades and then transferred through a gearbox and the rotor hub to the mechanical energy in shaft. The shaft drives the generator to convert the mechanical energy to electrical. The turbine model is based on the output power characteristics, expressed as [3][8]:

$$P_m = C_p(\lambda,\beta)\cdot\frac{1}{2}\rho A v_w^{\,3} \qquad (1)$$
$$\lambda = \frac{R_{blade}\omega_r}{v_w}$$

where P_m is the mechanical output power in watt, which depends on performance coefficient C_p, air density ρ, turbine swept area A and wind speed v_w. $(½)\cdot\rho A v_w^3$ is

978-1-4244-6395-4/10/$26.00 ©2010 IEEE

equal to the kinetic energy contained in the wind at particular speed v_w. The performance coefficient $C_p(\lambda, \beta)$, which depends on tip speed ratio λ and blade pitch angle β, determines how much of the wind kinetic energy can be captured by the wind turbine system. A nonlinear model describes $C_p(\lambda, \beta)$ as [8]:

$$C_p(\lambda,\beta) = c_1(c_2 - c_3\beta - c_4\beta^2 - c_5)e^{-c_6} \qquad (2)$$

where, c_1=0.5, c_2=116/λ_i, c_3=0.4, c_4=0, c_5=5, c_6=21/λ_i and

$$\frac{1}{\lambda_i} = \frac{1}{\lambda + 0.08\beta} - \frac{0.035}{\beta^3 + 1} \qquad (3)$$

where R_{blade} and ω_r are the blade radius and angular frequency of rotational turbine as depicted in Fig.1. The C_p-λ curve for this particular turbine model at different β, is shown in Fig.2 where illustrates that to achieve maximum C_p, one has β=0° and λ=8. The blade with fixed geometry will have fixed C_p-λ characteristics, as described in (2) and (3). Therefore, to track the optimal output power, the curve of P_m-ω_r is the "map" to follow. In this paper's wind turbine model, for different wind speeds and fixed β=0°, the P_m-ω_r curve is displayed in Fig.3 for wind speeds ranging from 6 m/s to 14 m/s. By connecting the maximum points of all curves, the relationship between maximum output power and the rotor speed can be proposed as:

$$P_{opt} = 0.5572\omega_r^3 - 0.5081\omega_r^2 + 0.4792\omega_r - 0.1449 \qquad (4)$$

This is the look-up table for optimal active power control in this paper.

III. SCIG Wind Power System

Fig. 4 shows the schematics of whole system including the wind turbine, pitch control and reactive power compensator. The entire system includes three stages for delivering the energy from wind turbine to the power grid. The first one is wind farm stage which handles with low-voltage V_{wt}; the second is distribution stage which has medium-voltage V_{dis}; the third is grid transmission stage which has high-voltage V_{grid}. The three-phase transformers take care of the interface between each stage other [9]. As mentioned, nominal power P_{nSCIG} is considered as active power reference to regulate the pitch angle while V_{dis} and I_{dis} denote the distribution line-to-line voltage and phase current and they are monitored to favor the reactive power compensation for distribution line. This fairly straightforward technique was firstly used since its simple, rugged construction, reliable operation and low cost. However, the fixed-speed essential and potential voltage instability problem severely limit the operations of wind turbine [1][3].

Since SCIG is of fixed speed generator, for a particular wind speed, the output active power is fixed as well. Thus, with the increase of wind speed, so does the output power until the nominal power is reached. The wind speed at this moment is called nominal wind speed. Beyond this speed, the pitch angle system will prevent the output power from exceeding the nominal value. That is, when the wind speed is below nominal value, the power capture can vary with the change of wind speed; when the wind speed is above nominal value, the pitch angle control system will limit the generated power by changing the pitch angle. In such way, the output power will be stabilized at nominal value at where the wind speed is always above nominal wind speed. The pitch angle is determined by an open-loop control of regulated output active power and, as shown in Fig. 5. Due to the huge size of blade thus inertia, pitch angle has to change in a slow rate and a reasonable range. It is also worthy to notice that without reactive power source, in section V, the SCIG system tends to lead to a voltage droop in distribution line which will cause overload problem. In simulation section, the comparison between SCIG system with and without STATCOM is conducted.

IV. DFIG Wind Power System

Traditionally, the dynamic slip control is employed to fulfill the variable-speed operation in wind turbine system, in which the rotor windings are connected with variable resistor and control the slip by varied resistance [3][10]. This type of system can achieve limited variations of generator speed but external reactive power source is still necessary. Consequently, to completely remove the reactive power compensation and control both active and reactive power independently, DFIG wind power system is one of most popular methods in wind energy applications [1][3][7]. This paper reproduces DFIG model first of all and then concentrates on the controlling schemes of power converters, in which the active and reactive power are controlled independently. Especially, the stator-side converter controlling involving a *RL* series choke is proposed. Both controlling of rotor- and stator-side converters voltages end up with a current regulation part and a cross-coupling part in this paper.

The wind turbine driving DFIG wind power system consists of a wound-rotor induction generator and an AC/DC/AC IGBT-based PWM converter (back-to-back converter with capacitor dc-link), as shown in Fig.6. In this configuration, the back-to-back converter consists of two parts: the stator/grid-side converter and the rotor-side converter. Both are voltage source converters applying IGBTs while a capacitor between two converters acts as a dc voltage source. The generator stator winding is connected directly to grid (with fixed voltage and frequency of grid) while the rotor winding is fed by rotor-side converter through slip rings and brushes, at variable frequency.

The control system is divided into two parts – stator-side converter control system and rotor-side converter control

system. An equivalent circuit of DFIG is depicted in Fig.7 and the relation equations for voltage V, current I, flux Ψ and torque T_e involve [4][11][12]:

$$V_{ds} = R_s I_{ds} - \omega_s \Psi_{qs} + \frac{d\Psi_{ds}}{dt} \qquad (5)$$
$$V_{qs} = R_s I_{qs} + \omega_s \Psi_{ds} + \frac{d\Psi_{qs}}{dt}$$

$$V_{dr} = R_r I_{dr} - s\omega_s \Psi_{qr} + \frac{d\Psi_{dr}}{dt} \qquad (6)$$
$$V_{qr} = R_r I_{qr} + s\omega_s \Psi_{dr} + \frac{d\Psi_{qr}}{dt}$$

$$\Psi_{ds} = L_s I_{ds} + L_m I_{dr} \qquad (7)$$
$$\Psi_{qs} = L_s I_{qs} + L_m I_{qr}$$

$$\Psi_{dr} = L_r I_{dr} + L_m I_{ds} \qquad (8)$$
$$\Psi_{qr} = L_r I_{qr} + L_m I_{qs}$$

$$T_e = \frac{3}{2} n_p (\Psi_{ds} I_{qs} - \Psi_{qs} I_{ds}) \qquad (9)$$

Where L_s=L_{ls}+L_m; L_r=L_{lr}+L_m; $s\omega_s = \omega_s - \omega_r$ represents the difference between synchronous speed and rotor speed; subscripts r, s and d, q denote the rotor, stator, d-axis and q-axis components respectively; T_e is electromagnetic torque; L_m, n_p, J are generator mutual inductance, the number of pole pairs and the inertia coefficient, respectively.

A. Rotor-side converter control

If the derivative parts in (5) are neglected, one can obtain stator flux as:

$$\Psi_{ds} = (V_{qs} - R_s I_{qs}) / \omega_s$$
$$\Psi_{qs} = (V_{ds} - R_s I_{ds}) / (-\omega_s) \qquad (10)$$
$$\Psi_s = \sqrt{\Psi_{ds}^2 + \Psi_{qs}^2}$$

Because of directly connected to the grid, the stator voltage shares constant magnitude and frequency of grid voltage. Ones could make the d-axis align with stator voltage vector, it is true that V_s=V_{ds} and V_{qs}=0, thus Ψ_s=Ψ_{qs} and Ψ_{ds}=0, which are of stator voltage oriented vector control scheme, as depicted in Fig. 8. According to equations (7) – (9), the rotor-side converter reference current is derived as:

$$I_{dr\_ref} = -\frac{2L_s T_e}{3n_p L_m \Psi_s} \qquad (11)$$

$$\text{Where } \begin{matrix} P_{e\_ref} = P_{opt} - P_{loss} = T_e \omega_r \\ P_{loss} = R_s I_s^2 + R_r I_r^2 + R_c I_{sc}^2 + F\omega_r^2 \end{matrix} \qquad (12)$$

Where I_{sc}, R_c and F are stator-side converter current, choke resistance and friction factor. P_{opt}, P_{e_ref} and P_{loss} are desired optimal output active power, reference active power and system power loss. Combining (10) - (12), the active power is used as command inputs to determine current references I_{dr_ref}. Meanwhile, the output reactive power is stator reactive output power since the stator-side converter's reactive power is set to be zero in this paper. Then, one has:

$$\begin{aligned} Q_o = Q_s + Q_{sc} = Q_s &= \mathbf{Im}[(V_{ds} + jV_{qs})(I_{ds} + jI_{qs})^*] = -V_{ds} I_{qs} \\ &= -V_{ds} \frac{1}{L_s} (\Psi_s - L_m I_{qr}) \end{aligned} \qquad (13)$$

Thus, the regulation of reactive power can lead to I_{qr_ref}, and then the rotor-side converter voltage signals $V_{dr}^{\ 1}$ and $V_{qr}^{\ 1}$ are derived by regulation of currents. In addition, the feedforward coupling part $V_{dr}^{\ 2}$ and $V_{qr}^{\ 2}$ are derived based on (6) and (8), as:

$$V_{dr}^{\ 2} = R_r I_{dr} - s\omega_s (L_r I_{qr} + L_m I_{qs}) \qquad (14)$$
$$V_{qr}^{\ 2} = R_r I_{qr} + s\omega_s (L_r I_{dr} + L_m I_{ds})$$

where the supercripts 1 and 2 denote the current regulation part and cross-coupling part respectively. At last, rotor-side converter voltage signals in d/q-axis are expressed as:

$$V_{drc} = V_{dr} = V_{dr}^{\ 1} + V_{dr}^{\ 2} \qquad (15)$$
$$V_{qrc} = V_{qr} = V_{qr}^{\ 1} + V_{qr}^{\ 2}$$

where subscript rc denotes the rotor-side converter. After the conversion of dq-abc, the rotor-side converter voltage V_{abc_rc} can be obtained. Fig.9 exhibits the control scheme for above procedure.

B. Stator-side converter control

Concerning of the use of three-phase series *RL* choke between stator and stator-side converter, a cross-coupling model is required to derive the voltage signal of stator-side converter, as described in Fig.10:

$$V_{dsc} = V_{ds} - V_{dch} \qquad (16)$$
$$V_{qsc} = V_{qs} - V_{qch}$$

where the subscript sc and ch denote the variables of stator-side converter and choke. The coupling part of voltage signals $V_{dch}^{\ 2}$ and $V_{qch}^{\ 2}$ are expressed as:

$$V_{dch}^{\ 2} = R_c I_{dsc} - \omega_s L_c I_{qsc} \qquad (17)$$
$$V_{qch}^{\ 2} = R_c I_{qsc} + \omega_s L_c I_{dsc}$$

Besides, $V_{dch}^{\ 1}$ and $V_{qch}^{\ 1}$ are determined by regulation of current I_{dsc} and I_{qsc} in which the current reference I_{qsc_ref} is given directly while I_{dsc_ref} is determined by the regulation of dc-link voltage V_{dc}. Thus, above all, the stator-side converter voltage signals V_{dsc} and V_{qsc} are obtained as following and depicted in Fig.11.

$$V_{dsc} = V_{ds} - V_{dch}{}^{1} - V_{dch}{}^{2}$$
$$V_{qsc} = V_{qs} - V_{qch}{}^{1} - V_{qch}{}^{2} \quad (18)$$

V. Simulation Results and Discussion

This section covers the simulation of two typical induction generator wind power systems. To manipulate the quantities in per unit (p.u.), the base values of power, voltage, speed and frequency are necessarily defined first of all. In this paper, the nominal power P_n (three phase), wind turbine bus voltage V_{wt} (phase-to-phase RMS value), synchronous speed ω_s and grid frequency f are chosen as base values. Other base values are obtained as:

$$\text{base current} = \frac{\frac{1}{3}\times \text{base power}}{\text{base voltage} \div \sqrt{3}} = \frac{\text{base power}}{\text{base voltage} \times \sqrt{3}} \quad (19)$$

$$\text{base impedence} = \frac{\text{base voltage} \div \sqrt{3}}{\text{base current}} = \frac{\text{base voltage}^2}{\text{base power}}$$

$$\text{base torque} = \frac{\text{base power}}{\text{base speed}}$$

$$\text{base flux linkage (RMS)} = \frac{\text{base voltage}}{\text{base frequencey} \times 2\pi}$$

The p.u. values of all quantities are given in:

$$p.u.\ \text{value} = \frac{\text{quantities in SI unit}}{\text{base value}} \quad (20)$$

Also, instead of specifying in kg*m^2, this paper defines the system inertia constant H in second as:

$$H = \frac{0.5 \times \text{inertia in SI unit} \times \text{base speed}^2}{\text{base power}} \quad (21)$$

A. SCIG System Simulation Results

A traditional 0.855 MW SCIG wind power system is developed in Matlab/Simulink. The related system data used are given in Table 1.

In order to investigate the system performances, a ramp wind speed (v_w) that varies from t = 10 sec. to t = 16 sec is assumed, and is then it maintained constant to the end of simulation at t = 40 sec. Figs. 12(a-e) show the dynamic variations and steady state results of the pitch angle β, the generator speed ω_r, the produced active power P and the consumed reactive power Q. The fluctuations in results during t = 0 and 2.5 sec. are due to the initial conditions. The response to the wind speed input disturbance is investigated with an initial speed of generator at slip s = -0.01 p.u., while all other initial values for power and voltages are zero. The steady-state results for v_w=8 m/s indicated the operation point: ω_r = 1.0015 p.u. and P = 0.29 MW. Since it is lower than nominal value 0.855 MW, indicates that pitch angle control is not working. After t = 10 sec., with the increase of v_w, ω_r and P until t = 13 sec. when v_w exceeds the nominal value (11 m/s). This is because the pitch control is triggered to limit the increase of output power P and Q as shown in Figs. 12 (b,c,d). In this way, the pitch control effectively limits the output P around nominal value 0.855 MW and settle a new pitch angle at roughly t = 17 sec. This nominal operation point can also be observed on Fig. 3 (v_w = 11 m/s; P = 0.855 MW; ω_r = 1.005 p.u.).

It is noted that the rotor speed can only vary in very small range around 1 p.u. (fixed-speed system) and thus impossible to achieve optimal active power output. Thus, the active power outputs at v_w = 8 m/s and ≥ 11 m/s in SCIG are 0.29 MW and 0.855 MW. Also, without independent control ability, SCIG system consumes reactive power 0.41 Mvar at final steady-state which will lead to line voltage droop. To provide necessary reactive power, a STATCOM is added on distribution line to investigate the improvement. As in Fig. 13, distribution line voltage can drop by 0.055 p.u. in SCIG system without STATCOM, which will be a potential induction of overload in system. In contrast, SCIG system with STATCOM can hold distribution voltage to 0.99p.u. , which produces favorable grid system stability. The compensated reactive power from STATCOM is shown in Fig. 14 and is equal to 0.3 Mvar at final steady-state, a little bit less than the real consumed value in Fig. 12(d). The STACOM provides impressive help on constant distribution line voltage. However, the DFIG presents better result and does not need the help from STACOM, as shown in Fig.13. Fig. 14 shows the STATCOM reactive power response.

B. DFIG System Simulation Results

The DFIG wind power system is simulated using the same turbine as in the SCIG system as well as the system parameters listed in Table 2. The DFIG system allows the optimal (maximum) output power operation in the absence of reactive power source. Also, independent control of active and reactive power is achieved.

In the Matlab/Simulink model, the converter switch frequency is set to be 27 times of grid frequency f. To achieve acceptable accuracy, discrete values of the power circuit and the control circuit models are taken at different time steps. It is worthy to note that the nominal apparent power and nominal active power are considered as nominal electrical power and nominal mechanical power in this wind power system [3][13]. Simulation and control system parameters are listed in Table 3 and are preloaded into workspace before running the simulation and easily to be modified in *m* file.

The steady-state results of system are shown in Fig.15 (a-d), which presents four wind speed cases v_w = 7, 9, 10, 12 m/s to verify the optimal power output tracking. All of them keep the bus voltage at 1200 VDC, indicating the well operation of stator-side converter while the reactive power is set to be zero as the input command. In order to track the optimal active power output, optimal rotor

speeds are implemented accordingly. For instance, one could recall Fig.3 that at v_w = 7 m/s, the optimal output active power is 0.17 p.u. of nominal power 1.5 MW, i.e. 0.255 MW. A little bit power droop could be observed from simulation results which are caused by power loss in (12). Meanwhile, the optimal rotor speed is also achieved at 0.75 p.u., same as the value in Fig.3. Similarly, the optimal tracking of output power and rotor speed is exhibited in other wind speed cases as well. Therefore, it can be concluded that the system works well to follow the optimal power control at steady-state operation. It is noticed that P and Q are vanished during the first cycle (1/60 sec) in displayed result because of the calculation time cost.

The system dynamic response to varied wind speed is investigated. Due to the large H of the system, dynamic variation can last and be observed in a long time period before converging to the steady-state values. To shorten such period, H = 0.1 sec. is used in this part of simulation. With stable steady-state initial values, three regular types of wind speeds are examined for dynamic responses, including step, ramp and gusty wind. The varied winds and corresponding results for V_{dc}, ω_r, P and Q are shown in Fig. 16-18, where the system can always reach a new optimal steady-state after a few seconds. In above results, the reduced inertia constants can only decrease the converging time, making system reach new steady-state quicker and it has no effects on steady-state values.

The system dynamic response to a grid disturbance is investigated. At v_w = 9 m/s, a remote voltage droop in grid is programmed from t = 0.09 sec. to 0.29 sec. The dynamic responses are presented in Fig. 19. During this process, since the wind speed remains the same, control system effectively makes the system recovers in approximate 0.1 sec.

VI. CONCLUSIONS

A SCIG and a DFIG wind power systems are modeled and simulated in Matlab/Simulink. An optimal active power versus rotor speed relationship is proposed for the wind turbine model, which functions as a look-up table for tracking the maximum output active power. The SCIG system presents requires external reactive power source to support grid voltage and it can keep the output power at the nominal level by pitch control but cannot change the rotor speed to achieve maximum wind power capture at different wind speed. In contrast, the DFIG system does not need reactive power compensator to hold distribution line voltage and achieves optimal active power controlling. A cross-coupling model between stator-side converter and a three phase choke is presented. The voltage control schemes for two converters consisted of a current regulation part and a cross-coupling part. The steady-state and dynamic responses for two systems are examined. It is concluded that the variable-speed wind power system has capability of optimal power control thus higher efficiency in wind power extraction.

References

1. M. Orabi, T. Ahmed, M. Nakaoka, "Efficient performances of induction generator for wind energy utilization", IEEE 30th Annual Conf. Indus. Elec. Society, pp. 838-843, Nov. 2004.
2. M. Molinas, Jon Are Suul and T. Undeland, "Low voltage ride through of wind farms with cage generators: STATCOM Versus SVC", IEEE Trans. on Power Electronics, vol. 23, no. 3, pp. 1104-1117, May 2008.
3. Z. Chen, J. M. Guerrero and F. Blaabjerg, "A review of the state of the art of power electronics for wind turbines", IEEE Trans. on Power Electronics, vol. 24, no. 8, pp. 1859-1875, Aug. 2009.
4. Y. Lei, A. Mullane and G. Lightbody, "Modeling of the wind turbine with a doubly fed induction generator for grid integration studies", IEEE Trans. on Energy Conversion, vol. 21, no. 1, pp. 257-264, Mar. 2006.
5. R. Ganon, G. Sybille and S. Bernard, "Modeling and real-time simulation of a doubly-fed induction generator driven by a wind turbine", Int. Conf. Power Systems Transients, pp. 162-169, June 2005.
6. H. Sun, Y. Ren and H. Li, "DFIG wind power generation based on back-to-back PWM converter", IEEE Proceedings Int. Conf. Mechatronics and Automation, pp. 2276-2280, Aug. 2009.
7. L. X, P. Cartwright, "Direct active and reactive power control of DFIG for wind energy generation", IEEE Trans. on Energy Conversion, vol. 21, no. 3, pp. 750-758, Sept. 2006.
8. S. Heier, *Grid Integration of Wind Energy Conversion Systems*, John Wiley & Sons, 2006.
9. N. W. Miller, W. W. Price and J. J. Sanchez-Gasca, "Dynamic modeling of GE 1.5 and 3.6 wind turbine-generators", GE Power Systems, Oct. 2003.
10. R. Pena, J. C. Clare and G. M. Asher, "Doubly fed induction generator using back-to-back PWM converters and its application to variable-speed wind-energy generation", IEE Proc.-Electr. Power Appl. vol. 143, no. 3, pp. 231-241, May 1996.
11. Feijo, J. Cidrs, and C. Carrillo, "Third order model for the doubly-fed induction machine", Elect. Power Syst. Res., vol. 56, pp. 121-127, Mar. 2000.
12. T. Ghennam, E. M. Berkouk, and B. Francois, "DC-link voltage banlancing algorithm using a space-vector hysteresis current control for three-level VSI applied for wind conversion system", Power Elect. and Appl. European conf., pp. 1-10, Sept. 2007.
13. M. Stiebler, *Wind Energy Systems for Electric Power Generation*, Springer, Germany, 2008.

Table 1 SCIG based Wind Power System Parameters

Parameter	Value
Nominal Wind Speed V_w	11 m/s
Nominal Active Power P_{nSCIG}	0.855 MW
Grid Voltage V_{grid}	120 kV
Grid Frequency f_{grid}	60 Hz
Distribution Line Voltage V_{dis}	12.5 kV
Wind Turbine Bus Voltage V_{wt}	575 V
Stator Resistance R_s	0.0048 p.u.
Stator Leakage Inductance L_s	0.1248 p.u.
Rotor Resistance R_r	0.0044 p.u.
Rotor Leakage Inductance L_r	0.1791 p.u.
Mutual Inductance L_m	6.77 p.u.
STACOM Constant Voltage V_{dc}	4 kV
STACOM Equivalent Capacitance C	625 μF

Table 2 DFIG based Wind Power System Parameters

Parameter	Value
Nominal Wind Speed v_w	11 m/s
Nominal Apparent Power S_e	1.67 MVA
Nominal Active Power P_{nDFIG}	1.5 MW
Power Factor pf	0.9
Grid Voltage V_{grid}	120 kV
Grid Frequency f	60 Hz
Distribution Line Voltage V_{dis}	12.5 kV
Wind Turbine Bus Voltage V_{wt}	575 V
Generator Number of Pole Pairs n_p	3
Stator Resistance R_s	0.0071 p.u.
Stator Leakage Inductance L_s	0.171 p.u.
Referred Rotor Resistance R_r	0.005 p.u.
Referred Rotor Leakage Inductance L_r	0.156 p.u.
Stator-to-Grid Coupling Resistance R_c	0.003 p.u.
Stator-to-Grid Coupling Inductance L_c	0.3 p.u.
Mutual Inductance L_m	2.9 p.u.
Nominal DC-link Voltage V_{dc}	1.2 kV
DC-link Capacitance C	10 mF
Maximum Current rating of Converter I_{conv_max}	0.5 p.u.
System Inertia Coefficient H	5 second
Generator Friction Damping F	0.01 p.u.

Table 3 Simulation and Control Parameters

Parameter	Value
Power System Sampling Period T_{s_Power}	5e-6 sec
Control System Sampling Period $T_{s\_Control}$	1e-4 sec
Switch Frequency f_{sw}	1620 Hz
Transmission Distance D_{tran}	30 km
Reactive Power Regulator Coefficients K_p; K_i	0.05; 5
DC-link Voltage Regulator Coefficients K_p; K_i	0.002; 0.1
Rotor-side Converter Current Regulator Coefficients K_p; K_i	0.3; 8
Stator-side Converter Current Regulator Coefficients K_p; K_i	2.5; 500

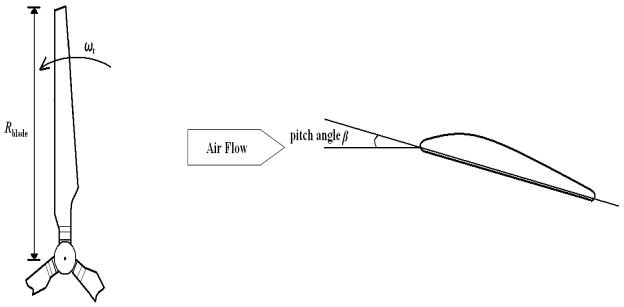

Fig.1 Schematics of turbine blade from different views

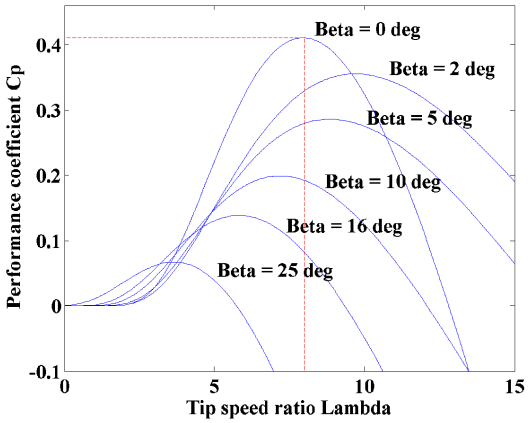

Fig. 2 C_p-λ curve for the turbine model

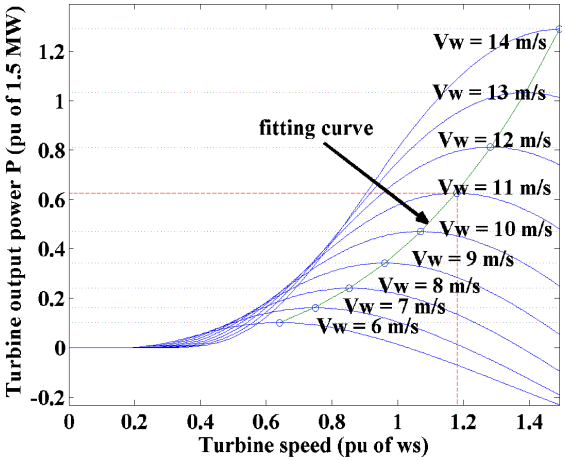

Fig. 3 P_m-ω_r curve for the turbine model

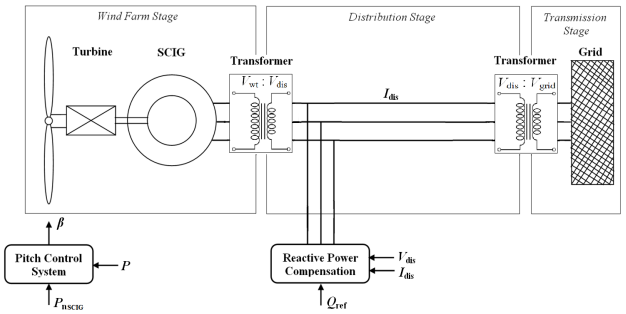

Fig. 4 SCIG wind power system topology

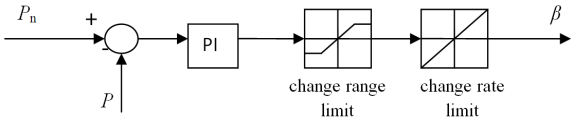

Fig. 5 Pitch angle control

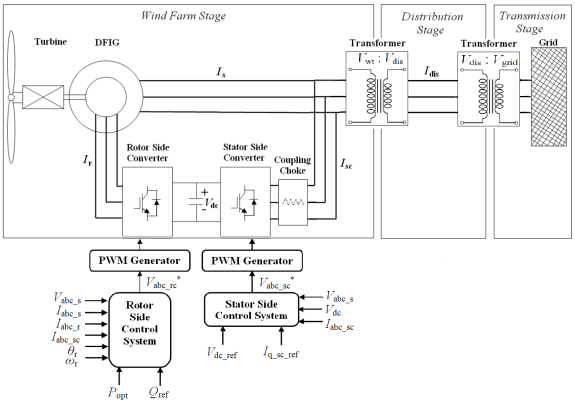

Fig. 6 WT-DFIG system configuration

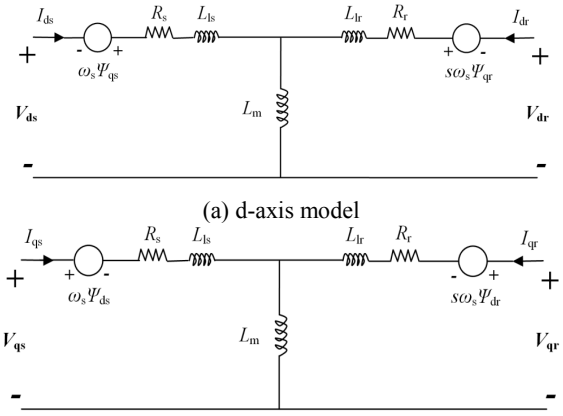

(a) d-axis model

(b) q-axis model

Fig.7 Equavilent circuit of DFIG

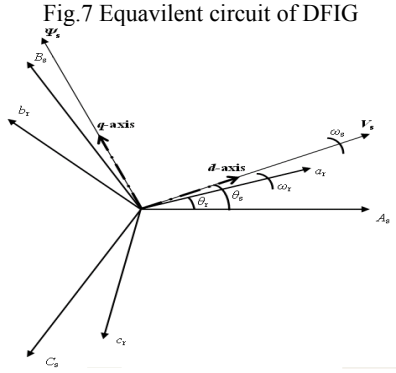

Fig.8 Stator voltage FOC reference frame

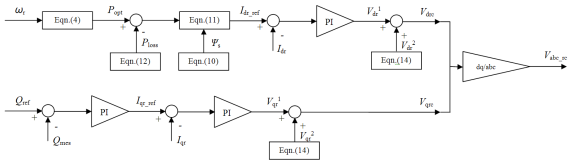

Fig.9 Rotor-side converter control scheme

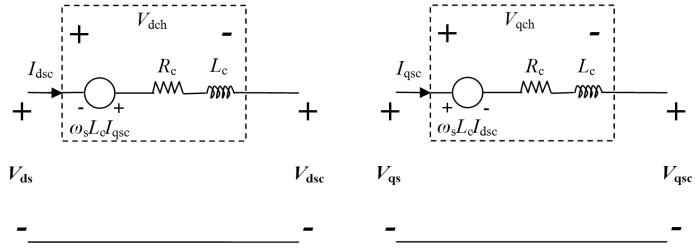

(a) d-axis model; (b) q-axis model

Fig.10 Equavilent circuit of stator-side-converter choke

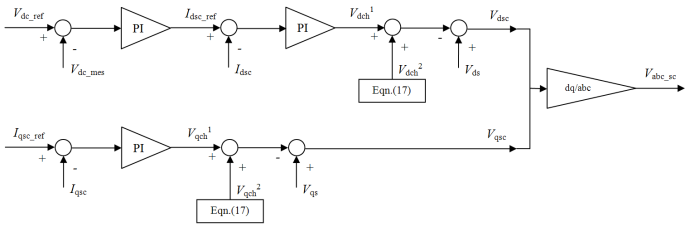

Fig.11 Stator-side converter control scheme

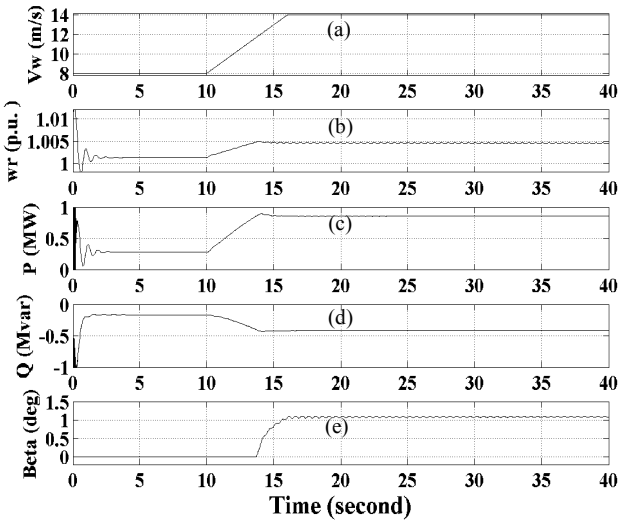

Fig. 12 Simulation results for SCIG system: (a) Wind speed v_w; (b) Generator speed ω_r; (c) Active power P; (d) Reactive power Q; (e) Pitch angle β;

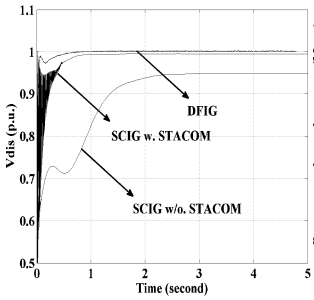

Fig. 13 Distribution voltage for SCIG system with/without STATCOM and DFIG system

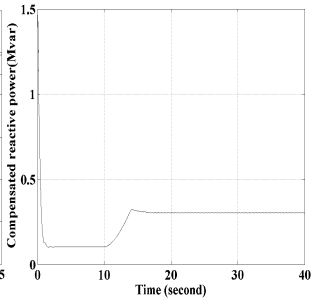

Fig. 14 STATCOM reactive power

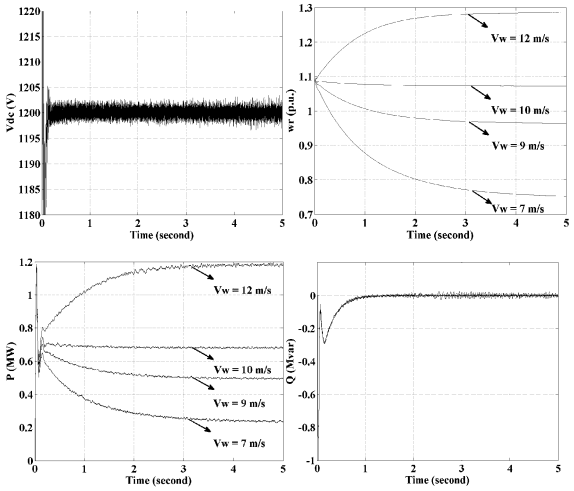

Fig. 15 System responses to different constant wind speed ((a) DC-link voltage V_{dc}; (b) Rotor speed ω_r; (c) Active power P; (d) Reactive power Q)

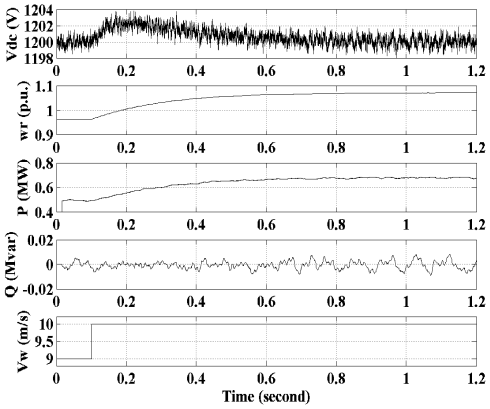

Fig. 16 Wind Step response ((a) DC-link voltage V_{dc}; (b) Rotor speed ω_r; (c) Active power P; (d) Reactive power Q; (e) Wind speed v_w;)

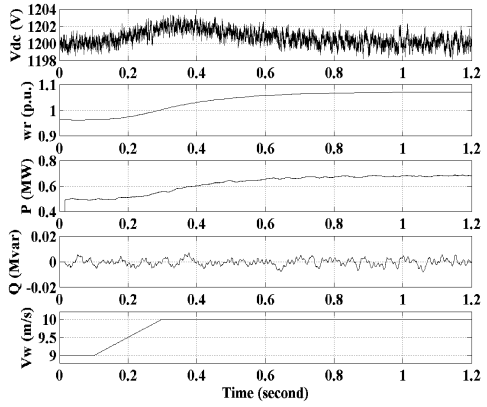

Fig. 17 Ramp wind response ((a) DC-link voltage V_{dc}; (b) Rotor speed ω_r; (c) Active power P; (d) Reactive power Q; (e) Wind speed v_w;)

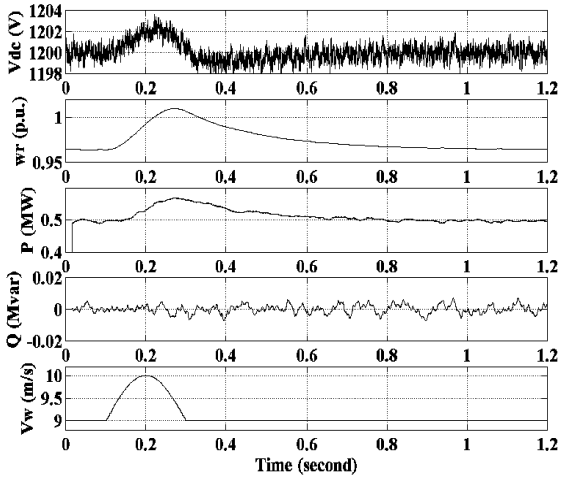

Fig. 18 Gusty wind response ((a) DC-link voltage V_{dc}; (b) Rotor speed ω_r; (c) Active power P; (d) Reactive power Q; (e) Wind speed v_w;)

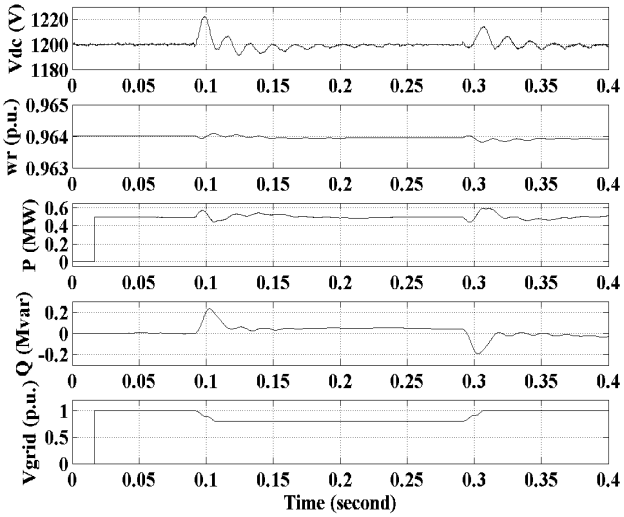

Fig. 19 Dynamic responses to grid voltage droop ((a) DC-link voltage V_{dc}; (b) Rotor speed ω_r; (c) Active power P; (d) Reactive power Q; (e) Grid voltage V_{grid};)